

12-26-2012

Polymorphism and polyamorphism in bilayer water confined to slit nanopore under high pressure


Jaeil Bai

University of Nebraska-Lincoln

Xiao Cheng Zeng

University of Nebraska-Lincoln, xzeng1@unl.edu

Follow this and additional works at: <http://digitalcommons.unl.edu/chemzeng>

 Part of the [Analytical Chemistry Commons](#), [Materials Chemistry Commons](#), and the [Physical Chemistry Commons](#)

Bai, Jaeil and Zeng, Xiao Cheng, "Polymorphism and polyamorphism in bilayer water confined to slit nanopore under high pressure" (2012). *Xiao Cheng Zeng Publications*. 132.

<http://digitalcommons.unl.edu/chemzeng/132>

This Article is brought to you for free and open access by the Published Research - Department of Chemistry at DigitalCommons@University of Nebraska - Lincoln. It has been accepted for inclusion in Xiao Cheng Zeng Publications by an authorized administrator of DigitalCommons@University of Nebraska - Lincoln.

Polymorphism and polyamorphism in bilayer water confined to slit nanopore under high pressure

Jaeil Bai and Xiao Cheng Zeng¹

Department of Chemistry, University of Nebraska, Lincoln, NE 68588

Edited* by Ho-kwang Mao, Carnegie Institution of Washington, Washington, DC, and approved November 19, 2012 (received for review August 2, 2012)

A distinctive physical property of bulk water is its rich solid-state phase behavior, which includes 15 crystalline (ice I–ice XIV) and at least 3 glassy forms of water, namely, low-density amorphous, high-density amorphous, and very-high-density amorphous (VHDA). Nanoscale confinement adds a new physical variable that can result in a wealth of new quasi-2D phases of ice and amorphous ice. Previous computer simulations have revealed that when water is confined between two flat hydrophobic plates about 7–9 Å apart, numerous bilayer (BL) ices (or polymorphs) can arise [e.g., BL-hexagonal ice (BL-ice I)]. Indeed, growth of the BL-ice I through vapor deposition on graphene/Pt(111) substrate has been achieved experimentally. Herein, we report computer simulation evidence of pressure-induced amorphization from BL-ice I to BL-amorphous and then to BL-VHDA₂ at 250 K and 3 GPa. In particular, BL-VHDA₂ can transform into BL-VHDA₁ via decompression from 3 to 1.5 GPa at 250 K. This phenomenon of 2D polyamorphic transition is akin to the pressure-induced amorphization in 3D ice (e.g., from hexagonal ice to HDA and then to VHDA via isobaric annealing). Moreover, when the BL-ice I is compressed instantly to 6 GPa, a new very-high-density BL ice is formed. This new phase of BL ice can be viewed as an array of square ice nanotubes. Insights obtained from pressure-induced amorphization and crystallization of confined water offer a guide with which to seek a thermodynamic path to grow a new form of methane clathrate whose BL ice framework exhibits the Archimedean 4·8² (square-octagon) pattern.

bilayer water and ice | molecular dynamics simulation | bilayer methane hydrate | amorphous-to-amorphous transition

The special character of confined water stems not only from unique properties of a hydrogen-bonding network, such as its ability to expand when cooled below the freezing point or to form rich structures of polymorphs under strong compressions, but from its spatial inhomogeneity, particularly in the nanoscale spaces. Forced to pack into the nanoscale spaces severely constricted by confining surfaces, water molecules in the vicinity of a flat surface tend to arrange themselves in layers parallel to the surface. The resulting oscillations in local density are reflected in properties of the confined water that can differ drastically from those of the bulk water. Not only are intriguing properties of confined water of fundamental interest, but they have implications for diverse practical phenomena at the intersection between chemistry, biological sciences, engineering, and physics: boundary lubrication in nano-fluidic and laboratory-on-a-chip devices; frost heaving in soil; synthesis of antifreeze proteins for ice-growth inhibition; rapid cooling of biological suspensions or quenching emulsified water under high pressure; storage of gas hydrates; and hydrogen fuel cells that generate electricity by passing hydrogen ions across a membrane, where water is confined in nanoscale channels. Hence, an improved understanding of the behavior of confined water could have practical benefits in addition to advancing basic science, such as better understanding of polymorphic transition at low dimension.

Polymorphism and polyamorphism refer to the existence of multiple crystalline and (metastable) amorphous states for homogeneous solid material, such as bulk ice (1–11). Mishima et al. (3) were the first to demonstrate that the high-density amorphous

(HDA) ice can be achieved through pressure-induced amorphization of either hexagonal ice, I_h, or low-density amorphous (LDA) ice at 77 K and 1 or 0.6 GPa. Later, Loerting et al. (6) uncovered a very-high-density amorphous (VHDA) ice, produced via isobaric heating of HDA from 77 to 165 (or 177) K at a pressure of 1.1 (or 1.9) GPa. More recently, Loerting et al. (9) observed a sequence of polyamorphic transitions (i.e., LDA → HDA → VHDA) at 125 K, starting from an LDA sample that is subjected to stepwise increasing pressure from 0.025 to 1.5 GPa. This was the first report of stepwise amorphous-to-amorphous-to-amorphous transitions. As elucidated by Debenedetti (11), a deeper insight into polyamorphic transitions of ice is required not only “for understanding phase behavior of water, but for the physics of disordered systems in general.”

A question that arises is the following: Can the polyamorphic transition occur in confined water/ice systems? For water confined to cylindrical pores (quasi-1D confinement), two recent experiments have demonstrated the existence of the low-density liquid (LDL) and prominent density hysteresis phenomenon, suggesting the possible existence of a first-order liquid–liquid phase transition in supercooled water (12, 13). Evidence of amorphous-to-amorphous transition in quasi-1D pores, however, has not been observed either from experiments or simulations. For water confined to quasi-2D slit pores with smooth walls and a width <6 Å, two distinctive crystalline forms of monolayer (ML) ice have been reported based on computer simulations, namely, the Archimedean 4·8² monolayer low-density ice (ML-LDI) and the puckered square monolayer high-density ice (ML-HDI) (14, 15). Such ML-LDI has also been found as a stable structure on a hydroxylated silica surface, but it is not free-standing due to strong interaction between water and the hydrophilic surface (16). However, no evidence of ML amorphous ice has been reported in the literature, suggesting that the glassy forms of ML water are unlikely to occur. In stark contrast to ML water, previous computer simulations have shown that numerous bilayer (BL) ices (or polymorphs) can be formed when a BL water is confined between two flat hydrophobic plates about 7–9 Å apart; for example, the BL-hexagonal ice (17–21), BL-Cairo pentagonal ice (22), BL-mixed pentagon hexagonal ice (22), BL-quasicrystal ice with 12-fold symmetry (22), BL-amorphous (BL-A) (21), and BL-VHDA₁ (23). In particular, a BL water can easily be turned into a BL-A ice within 200–270 K when the width of slit pore is fixed (in a range of 7–9 Å), as shown from previous computer simulations (21–24). Depending on the width of the slit pore and the magnitude of the lateral pressure, the density of the BL-A can be either lower or higher than that of BL liquid water. Note that the BL-A ice is a metastable phase, whereas the BL hexagonal ice (or BL-ice I) (17–25) is the thermodynamically stable phase in the slit pore when the lateral

Author contributions: J.B. and X.C.Z. designed research, performed research, contributed new reagents/analytic tools, analyzed data, and wrote the paper.

The authors declare no conflict of interest.

*This Direct Submission article had a prearranged editor.

¹To whom correspondence should be addressed. E-mail: xczen@phase2.unl.edu.

This article contains supporting information online at www.pnas.org/lookup/suppl/doi:10.1073/pnas.1213342110/-DCSupplemental.

pressure is less than 1 GPa. This is because BL-ice I can be obtained by annealing the BL-A through repeated cycles of cooling and heating (24).

Results and Discussion

We first demonstrate a polymorphic transition from the BL-ice I to a new VHDA at 250 K (akin to the pressure-induced bulk ice I_h to HDA transition). At 0 GPa lateral pressure and 250 K, a BL liquid water can freeze spontaneously into the BL-A (21, 24). Subsequent annealing of the BL-A for 20 ns yields the hexagonal BL-ice I, indicating BL-A is metastable with respect to BL-ice I. Next, we increase the lateral pressure from 0 to 4 GPa in several steps onto the BL-ice I. A sharp transition is observed at 2.9 GPa (Fig. 1A), and the new high-pressure phase is the BL-VHDA₂ whose structure can be viewed as antistacked parallelograms (Fig. 1B and Fig. S1B and D). Moreover, if the VHDA₂ is decompressed stepwise from 3 to 0.5 GPa at 250 K, it turns into BL-A below 1 GPa. Contrary to the BL-A \leftrightarrow VHDA₂ transition, which appears to be strongly first order due to the large hysteresis, the bulk LDA \leftrightarrow HDA transition has been viewed as “apparently first-order” (3),

whereas the bulk HDA \leftrightarrow VHDA transition may be viewed either as a first-order or kinetic densification (7), because the true nature of the first-order transition between bulk LDA, HDA, and VHDA is still under debate (9). Note also that unlike the BL-A, which satisfies the ice rule (i.e., every water molecule is hydrogen-bonded to exactly four nearest neighbor water molecules) (21), a hallmark for the BL-VHDA ices, such as BL-VHDA₁ reported previously (23) or BL-VHDA₂ as observed here, is that the ice rule is not satisfied (Fig. 1B). Also, importantly, if the BL-VHDA₂ is decompressed instantly from 3 to 1.5 GPa at 250 K, it turns into BL-VHDA₁ spontaneously, as shown in Fig. 1C (Movie S1). Unlike VHDA₂, which exhibits a structure of antistacked parallelograms, VHDA₁ exhibits a pentagon-based structure (23) (Fig. S1C and E). At 250 K and 1.5 GPa, not only is the potential energy of VHDA₁ lower than that of VHDA₂ (Fig. 1C), but the spontaneous transformation of VHDA₂ \rightarrow VHDA₁ suggests VHDA₁ is thermodynamically more stable than VHDA₂. Moreover, if VHDA₁ is compressed instantly from 1.5 to 3.0 or 6.0 GPa, it still maintains the pentagon-based structure, at least within 80 ns of simulation. Note that the computed diffusion constant for VHDA₁ and VHDA₂

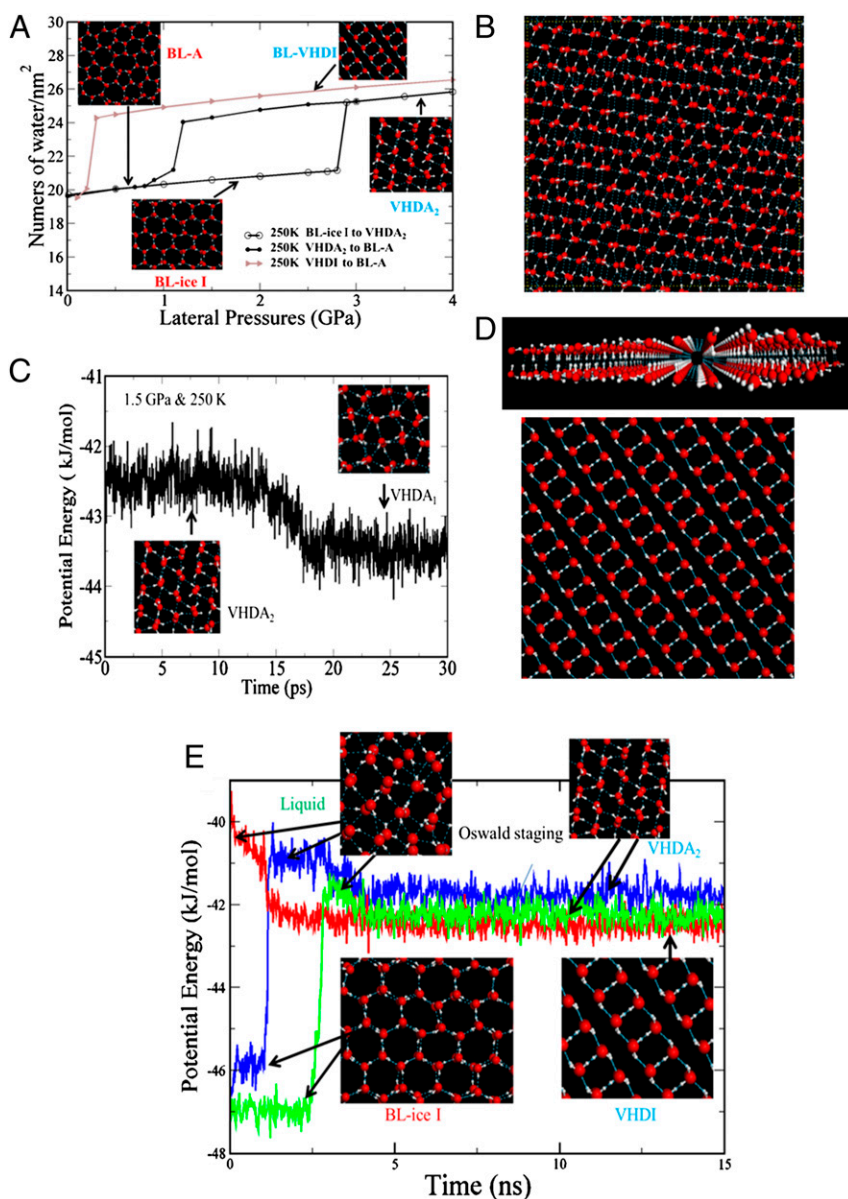


Fig. 1. (A) Isotherms (250 K) of BL water confined to a hydrophobic slit pore (with width $h = 8 \text{ \AA}$). Lines with open or filled symbols refer to the compression or decompression process in the lateral direction. (B) Top view of the BL-VHDA₂. (C) Time-dependent potential energy of the VHDA systems under instant decompression from 3.0 to 1.5 GPa at 250 K. (Insets) VHDA₂ and VHDA₁. The latter is composed of pentagons (Fig. S1C). (D) Side (Upper) and top (Lower) views of BL-VHDI. Color code: O, red; H, white; hydrogen bond, blue dotted line. (E) Red lines refer to time-dependent energy and show a phase transition from BL-ice I to BL-VHDI via compressing BL-ice I instantly from 0 to 6 GPa at 250 K; green lines (compression from 0 to 2.9 GPa in 100-MPa step at 250 K) and blue lines (compression from 0 to 2.8 GPa in 100-MPa step at 270 K) refer to time-dependent energy during the phase transition from BL-ice I to VHDA₂ via stepwise compression.

is $\sim 8 \times 10^{-9} \text{ cm}^2/\text{s}$ and $5 \times 10^{-9} \text{ cm}^2/\text{s}$ (at 250 K and 2 GPa), respectively, whereas the computed diffusion constant of BL water is $\sim 6 \times 10^{-6} \text{ cm}^2/\text{s}$ (at 280 K and 0.5 GPa), about three orders of magnitude larger.

In addition to the VHDA₂, a new very-high-density crystalline ice (VHDI) is obtained through an instant lateral compression from 0 to 6 GPa on the BL-ice I at 250 K. As shown in Fig. 1D, the structure of the VHDI can be viewed as an array of square ice nanotubes. Within each square ice nanotube, the ice rule is satisfied, as is the case for all BL crystalline ices reported thus far. The computed diffusion constant for VHDI is $\sim 3 \times 10^{-10} \text{ cm}^2/\text{s}$ (at 250 K and 2 GPa), which is slightly smaller than that of VHDA₁ and VHDA₂. The brown isotherm in Fig. 1A demonstrates the inverse polymorphic transition from VHDI to BL-A at 0.3 GPa under a lateral decompression at 250 K. Here, the large hysteresis indicates that the BL-VHDI can be (meta)stable over a wide range of pressure (from 0.3 to 6 GPa). Note that the transition from the BL-ice I to VHDI or to VHDA₂ exhibits the Oswald staging phenomenon; namely, an intermediate liquid state arises during the solid-to-solid transition (Fig. 1E and Movies S2 and S3). In the middle Oswald stage, the diffusion constant of water increases up to $8 \times 10^{-7} \text{ cm}^2/\text{s}$ and stays above $10^{-7} \text{ cm}^2/\text{s}$ for 0.5–1.5 ns. Thereafter, the diffusion constant decreases gradually toward that of solid phases on freezing. The Oswald staging phenomenon was previously observed in the transition from the ML-LDI to ML-HDI (24).

To gain more insight into the structural features of the VHDA_s and VHDI, site-site radial distribution functions (RDFs) are plotted (see Fig. 2). Owing to the long-range order, all RDFs of the VHDI show features of sharp peaks. In particular, the oxygen (O)-hydrogen (H) RDF of the VHDI can be used to understand hydrogen-bond ordering and violation of the ice rule (Fig. 2C). The arrow in Fig. 2C refers to the cutoff distance (2.2 Å) to define intrasquare ice nanotube hydrogen bonds. All sharp peaks located left of the arrow correspond to the hydrogen bonds within each square ice nanotube, which satisfies the ice rule. Major peaks located between 2.3 and 2.5 Å correspond to the intersquare nanotube hydrogen bonds, whose length is typically between 2.3 and 2.5 Å (Fig. S14). These intertube hydrogen bonds are weaker compared with intratube hydrogen bonds whose length is < 2.2 Å. The hydrogen-bond arrangement in VHDI suggests that the ice rule still plays an important role in the formation of ice structures under

very high pressure. The O-O RDFs of VHDA₂ (both inherent structure and structure at 250 K) indicate strong short-range order, but the long-range order disappears as the radial distance increases. This is very similar to the O-O RDFs of VHDA₁ reported by Han et al. (23) (Fig. 2). The O-H RDFs indicate that the hydrogen-bond lengths in VHDA_s are typically less than 2 Å and the distribution of O-H RDF distances of VHDA₂ and VHDA₁ are quite similar to one another (Fig. 2C). Overall, the O-O RDFs confirm that VHDA structures indeed lack the long-range order, and the transition from BL-ice I to VHDA₂ is a strong first-order polymorphic transition, whereas the transition from BL-ice I to VHDI is a strong first-order polymorphic transition.

To achieve better understanding of the polymorphic transition of BL water, isotherms (290 and 300 K) are displayed as a function of lateral pressure in Fig. 3A. Here, the green-square line shows a smooth transition from a BL liquid to VHDA₂ at ~ 3.1 GPa at 300 K. At relatively low pressures (< 0.5 GPa), the densities of a BL liquid are increased at a faster rate during the compression, whereas in the region of 0.5–3 GPa, the densities increase more slowly. Near 3.1 GPa, the number densities of liquid and VHDA₂ are very close to each other. Beyond 3.1 GPa, the densities of VHDA₂ follow the green-square line up to 4 GPa. Hence, the VHDA₂ appears to be a continuous densification of liquid on compression at 300 K. The orange-triangle line in Fig. 3 shows a sharp phase transition from the BL-ice I to a BL liquid at ~ 1.1 GPa and 300 K. Like bulk ice I_h, which has a lower density than bulk water, the BL-ice I also has an area density much lower than that of BL liquid under high lateral pressure. Overall, the three 300-K isotherms in Fig. 3 exhibit a sequence of crystal-to-liquid-to-amorphous transition. The blue-diamond line in Fig. 3 shows a sharp phase transition at ~ 2.2 GPa and 290 K from the VHDA₂ to a BL liquid under stepwise decompression. Subsequent to the phase transition, the liquid density decreases continuously under further decompression, following exactly an inverse path of the green-square line. Evidence of the first-order liquid-to-liquid (or BL-HDL-to-BL-LDL) transition is not observed for the BL water (26). The purple-diamond line in Fig. 3 represents decompression of the VHDI at 300 K, which leads to the melting of VHDI at ~ 1 GPa. Fig. 3B displays a schematic phase diagram of three stable phases, BL-ice I, VHDI, and BL liquid, constructed based on Figs. 1A and 3A and complementary

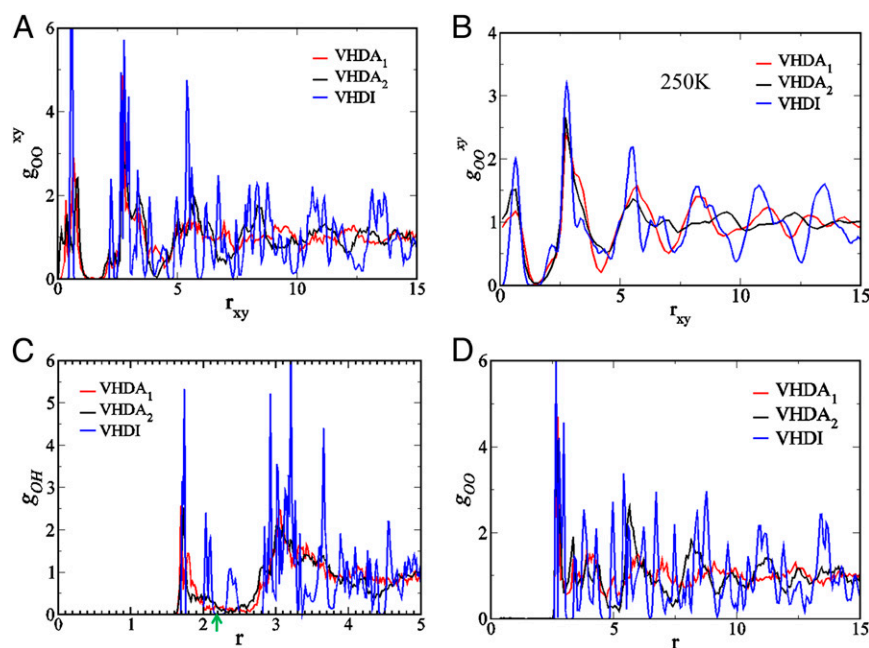


Fig. 2. RDFs of compressed BL-VHDI, BL-VHDA₁, and BL-VHDA₂. Projected O-O RDFs (inherent structures) (A), projected O-O RDFs of the BL structures at 2 GPa and 250 K (B), short-range O-H RDFs (inherent structures) (C), and O-O RDFs (inherent structures) (D). The arrow in C denotes the cutoff distance; the peaks on the left of the green arrow correspond to hydrogen bonds within each square ice nanotube, which satisfy the ice rule. (Inherent structures have a density corresponding to 2 GPa at 250 K.)

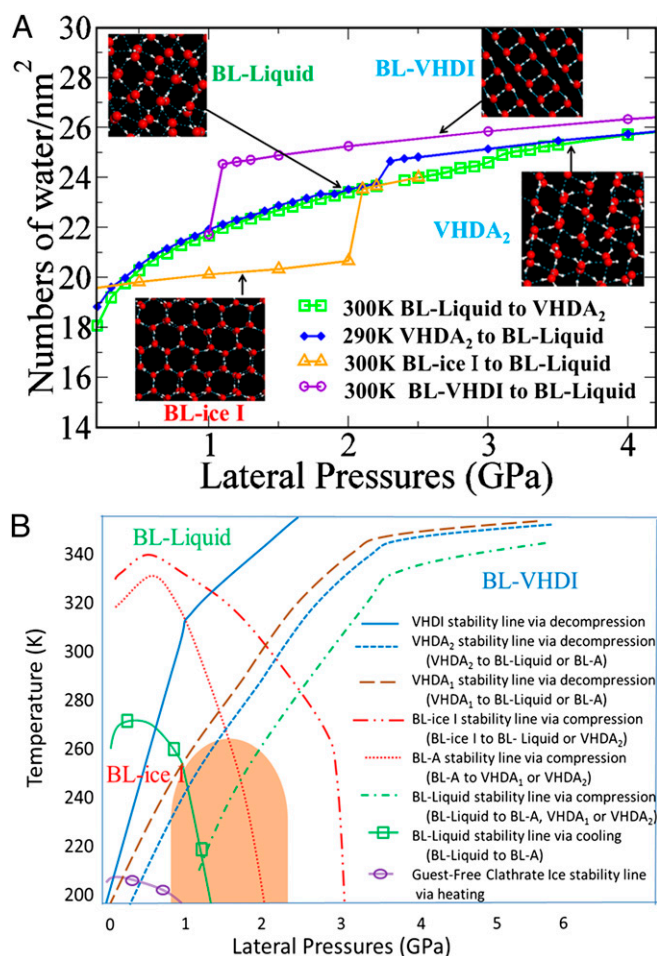


Fig. 3. (A) Isotherms of BL liquid water and BL-ice I confined to a hydrophobic slit pore (with width $h = 8 \text{ \AA}$). The purple-diamond, green-square, and orange-triangle lines refer to those of 300 K, and the blue-diamond lines refer to those of 290 K. Lines with open or filled symbols refer to the compression or decompression process, respectively, in the lateral direction. (B) Schematic lateral pressure-temperature phase diagram shows the location of three stable phases (BL-ice I, BL-VHDI, and BL liquid water). The red dotted-dashed line and blue solid line refer to stability lines of BL-ice I and BL-VHDI, respectively. The brown and blue dashed lines, and red-dotted line refer to metastability lines (or limits of metastability) of VHDA₁, VHDA₂, and BL-A, respectively. The green lines refer to the stability line of BL liquid water. The purple line refers to the metastability line of the BL-LDI with the Archimedean $4\cdot 8^2$ pattern (Fig. S2). The orange shade refers to a region with the possible existence of multiple metastable phases (BL-A, VHDA₁, and VHDA₂). As an example, in the orange shade region left to the red-dotted line, an amorphous-to-amorphous transition from BL-A to VHDA₁ is observed when the BL-A is under an instant compression to 1.6 GPa.

simulations. The stability lines of the stable phases and metastability lines of metastable amorphous phases are also estimated from the molecular dynamics (MD) simulation (15, 27) and shown schematically in Fig. 3B. The orange region between the two stable crystalline phases of BL-ice I and VHDI in Fig. 3B refers to the possible existence of multiple metastable phases. Here, the polyamorphism is plausible because the metastable phase is strongly path-dependent; namely, the final structure depends on the initial structure. In stark contrast, no such metastable phase region was found between the ML-LDI and ML-HDI phases for ML water (15).

Having demonstrated the formation of BL-VHDI and BL-VHDA₂, as well as polymorphic and polyamorphic transitions in the slit nanopore, we attempt to simulate spontaneous formation

of methane clathrate (MeC) (28–32) in the slit nanopore with guest methane molecules entrapped in octagons. A motivation of this specific simulation stems from our previous study of ML-MeC (15), for which we find that the guest-free ML ice clathrate is actually a low-density stable phase of ML ice (namely, ML-LDI). One may ask whether the guest-free BL ice clathrate would be a stable bilayer low-density ice (BL-LDI). To address this question, we first examine the stability of BL-MeC without any guest molecules. To this end, we construct a new BL ice by stacking two ML-LDIs (with the Archimedean $4\cdot 8^2$ pattern) on top of each other in registry. This BL ice has a lower density than the BL-ice I, and thus is a BL-LDI (Fig. S2A and E). The BL-LDI is optimized at zero temperature with a fixed volume in the slit nanopore. Subsequent to the structural optimization, an MD simulation in the canonical (NVT) ensemble is performed at several different temperatures. It turns out that the BL-LDI whose hydrogen-bonding network satisfies the ice rule is metastable up to 200 K (Fig. S2). When the temperature is in the range of 220–240 K, polygons other than square and octagon arise, and the BL-LDI is changed eventually to a solid structure consisting of domains of BL-ice I and cavities (Fig. S2D). The formation of cavities in the BL-ice I is largely due to the fixed-volume simulation wherein the BL-LDI cannot be converted to a perfect BL-ice I without changing the area of the simulation cell. We also perform the constant particle number, lateral pressure, constant slit width, and temperature ($NP_{xy}hT$) simulation, with the lateral pressure being zero. As expected, the area of the simulation cell is reduced when octagons are converted to hexagons and no cavities are formed (Fig. S2H).

Because the BL-LDI is thermodynamically unstable above 200 K, can the BL-LDI be stabilized by methane molecules? To pursue this possibility, we examine direct temperature quenching of BL liquid water/methane mixtures. As shown in Fig. S3, several different ratios of methane/water molecule (ranging from 0% to 12.5%) are considered. The mixtures are equilibrated at 1,000 K and 0.5 GPa and are then quenched instantly to 250 K at the same lateral pressure. As shown in Fig. S3F, the pure BL ice without methane is very similar to BL-ice I, confirming that the BL-LDI is unlikely to form at 250 K. For the mixture with 1.25% composition of methane (CH_4), water octagons are formed, each containing a CH_4 molecule (Fig. S3E), and the nucleation of octagons promotes further formation of empty water octagons. As the composition of CH_4 increases to 5% (Fig. 3C), more CH_4 -containing octagons are formed. When the composition of CH_4 is increased to 6.25%, interestingly, the number of water BL-pentagons becomes comparable to that of water BL-hexagons in the system. This trend suggests that adding a small fraction of CH_4 in a BL liquid promotes the formation of BL-LDA ice that contains small and random domains of water octagon-square structure, wherein a CH_4 molecule is trapped in the octagon. This mechanism is very similar to that of making hyperquenched glassy water via spraying water droplets onto an ultracold liquid, such as liquid propane at $\sim 80 \text{ K}$. With the largest composition (12.5%) of CH_4 considered (Fig. S3A), methane is supersaturated; thus, domains of liquid CH_4 can be observed during the quenching simulation for 40 ns (Movie S4). Nevertheless, there are still small and random domains of BL-LDI formed in the system, a sign of nucleation of BL-LDI.

To seek a thermodynamic path for achieving a near-perfect BL-MeC crystal (Fig. 4C), we also attempt four independent instant compressions of the mixed ice/ CH_4 structure (with the composition of CH_4 at 12.5%) at 250 K from 0.5 to 1.0, 1.5, 2, and 4 GPa, respectively. As shown in Fig. S4, none of the four simulation procedures gives rise to a near-perfect BL-MeC crystal. Lowering the temperature below 250 K produces little change in structure, whereas increasing the temperature can slightly promote the formation of octagon-square domain. Repeated compression/decompression and cooling/heating will only increase the size of octagon-square domain slightly.

Nevertheless, the emergence of the aforementioned water BL-pentagons offers a clue to finding a simulation procedure to produce near-perfect BL-MeC. The key is to remove BL-pentagons that favor amorphous rather than crystalline structure. Note that the BL-pentagon water cluster is energetically more stable than any other BL-polygonal water cluster. As shown in Fig. 4, we use a four-step simulation procedure, including cyclical heating/annealing, stepwise compression, and long-term incubation, which can remove most BL-polygon defects, BL-pentagons in particular, concomitant with the growth of octagon-square domains. To gain more insight into the strenuous simulation process required to grow a perfect BL-MeC, we perform a test $NP_{xy}T$ simulation at 300 K and 1 GPa for 160 ns as illustrated in Fig. S4A and B and Movie S10. Here, the simulation starts from an initial configuration of a phase-separated liquid water and CH_4 gas at 300 K and 10 MPa (Fig. S4A). When the lateral pressure is increased instantly to 1.0 GPa (Fig. S4B), nucleation of CH_4 -containing octagon can be observed even at a very early stage. However, the formed octagons can easily collapse until a nucleus of a critical size (consisting of at least four octagons) forms. As more CH_4 molecules are dissolved in the solid solution (becoming MeC), numerous pentagons start to form to connect the octagons. The formation of nexus BL-pentagons is responsible for obstruction of the growth of BL-MeC.

To some extent, the kinetic process required to grow a perfect BL-MeC illustrated above has some similarity to that involved in the computer simulation of the growth of bulk MeC (31). For the latter, the ice/ CH_4 mixture is compressed instantly from 0 to 22 MPa at 250 K, and the temperature and pressure are then increased up to 27.2 MPa and 272 K, respectively. Thereafter, the temperature and pressure of the mixture are increased along the nonlinear P - T curve, which includes a decompression process, above the ice-melting temperature and below the MeC dissociation temperature. Likewise, the present simulation shows evidence of solid-state deformation and superheating of BL-ice I during the formation of BL-MeC. Despite the differences in the phase boundary of bulk ice (I_h and III) and BL-ice (BL-ice I and BL-VHDI), the kinetic processes of bulk and BL-MeC formation show a similar trend. For example, the previous simulation study (32) reveals an unknown cage formed during the growth of bulk MeC, which is different from a known nexus cage. The unknown cages can cause adverse effects on the growth of MeC. A similar behavior exists in the growth of BL-MeC. Here, the highly stable

BL-pentagons tend to fill the space between BL-octagons to hinder the formation of BL-MeC. The BL-pentagons are smaller than BL-hexagons but larger than BL-tetragons. Like BL-tetragons, the BL-pentagons can maintain their structural integrity together with BL-octagons. The incubation at 320 K can remove the unwelcome BL-pentagons. Once they are removed, the BL-squares become the nexus cages to grow BL-MeC. Likewise, a certain strategy needs to be developed to remove the unknown nexus cage during the growth of bulk MeC.

The BL-MeC crystal is stable up to 330 K at zero pressure (i.e., the stability limit under heating), and it transforms into methane gas and liquid water at 340 K. To determine the melting temperature of the BL-MeC crystal $[(\text{H}_2\text{O})_8\text{CH}_4]$ at zero pressure more accurately, we use the two-phase coexistence simulation method with the constant particle number, lateral pressure, constant slit width, and enthalpy ($NP_{xy}hH$) ensemble (33). As shown in Fig. S5A, the computed melting temperature of BL-MeC is about 285 K. For comparison, the computed melting temperature of the BL-ice I is about 293 K (Fig. S5B).

Density profiles of oxygen and CH_4 in the z -direction (normal to the wall surface) are plotted in Fig. S4E and F. The distribution function of oxygen in the BL-MeC exhibits sharp peaks, a manifestation of solid state, whereas the distribution of oxygen atoms in the phase-separated liquid is broad. In contrast, the distribution function of methane in the BL-MeC is also broad but differs from that in the phase-separated liquid (Fig. S4E). The distribution function of methane at several different temperatures (Fig. S4F) indicates that methane molecules become less mobile in the z -direction as the temperature is lowered, but they are still not confined between two MLs until the temperature is below 50 K.

In conclusion, several stable and metastable BL ices and amorphous ices are found within a slit nanopore. Structural transitions among them provide clear simulation evidence of polymorphism and polyamorphism in BL water. Moreover, the BL-square water clusters are not only building blocks of VHDI at high pressure but become the nexus “cages” for connecting methane-containing BL-octagons to form the BL-MeC. Due to high stability of BL-pentagon water clusters, which tend to hinder the growth of BL-MeC, a strenuous simulation procedure is required to remove the BL-pentagons and to grow near-perfect BL-MeC. Finally, we remark that the network structure of BL-MeC can be viewed as a projection of the network structure of bulk methane hydrate

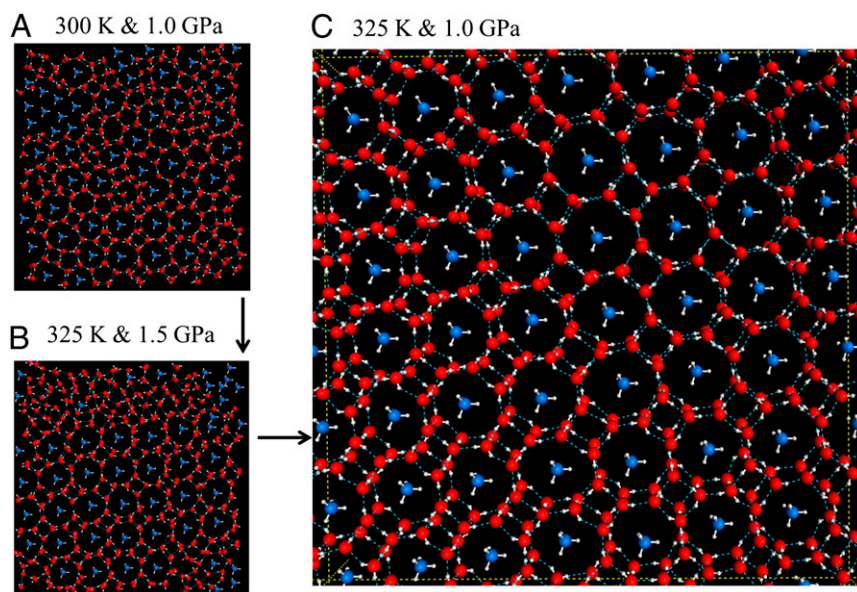


Fig. 4. Thermodynamic path designed in an MD simulation to grow the BL-MeC spontaneously. Specifically, starting from an ice/ CH_4 mixture structure as shown in Fig. S3A (obtained at 250 K and 0.5 GPa; Movie S4), the structure is heated instantly to 270 K and then goes through incremental step annealing and reheating cycles (270 \rightarrow 265 \rightarrow 260 \rightarrow 255 \rightarrow 250 \rightarrow 255 \rightarrow 260 \rightarrow 265 \rightarrow 270 K) for total 40 ns, for which each incremental step takes 1 ns. As a result, the water octagon-square domain grows gradually. At certain stage, the growth process stops due to high stability of BL-polygons (defects) in the structure. Next, the temperature and pressure of the system are raised instantly to 300 K and 1.0 GPa for 10 ns (Movie S5). (A) Top view of a snapshot of the methane-water mixture is shown. The temperature and pressure of the system are then raised instantly to 310 K and 1.5 GPa, respectively, for 10 ns (Movie S6), followed by a rise of temperature to 320 K for 20 ns (Movie S7) and to 325 K for 20 ns (Movie S8). (B) Top view of the final snapshot of the methane-water mixture is shown. Lastly, a long simulation (65 ns) is performed at 1.0 GPa and 325 K to achieve a perfect BL-MeC (Movie S9). (C) Top view of the inherent structure of the BL-MeC at 325 K and 1.0 GPa is shown. The slit pore width $h = 8$ Å in all simulations.

phase III (MH-III) along the direction normal to the octagon cages. It is known that MH-III is stable only at high pressures beyond 1.8 GPa (34). On the other hand, the BL-ice I can be viewed as a projection of bulk ice I_h in the direction normal to the puckered hexagons. Such a geometric connection between BL ices (ice clathrate) and their 3D counterparts suggests more qualitative connections in polymorphic and polyamorphic transitions for BL and bulk ices (clathrates) may exist, despite the strong effect of confinement with the BL water.

Materials and Methods

MD Simulation. The slit nanopore consists of two rigid and smooth hydrophobic walls. The wall-wall separation (width h) is set to be 8 Å, which can accommodate two MLs of water. The transferable-intermolecular-potentials-5-point-charge (TIP5P) water model is adopted (35). The 9-3 Lennard-Jones (LJ) potential is used to describe the water-hydrophobic wall interaction (15, 17, 21, 24). The MD simulations are performed using the $NP_{xy}hT$ ensemble. The periodic boundary conditions are applied in the lateral direction (x and y) in parallel with the two walls. The simulation supercell contains 400 water molecules with or without methane. A test simulation of the compression of BL-ice I is also performed with 800 water molecules at 250 K and 6 GPa. Spontaneous formation of BL-VHDI is observed, as in the case of using 400 molecules. No apparent size effect is detected.

The methane molecule is modeled by a united-atom model whose LJ parameters are $\sigma_{\text{methane}} = 3.758$ Å and $\epsilon_{\text{methane}} = 0.2959$ kcal/mol (15). The cross-interaction parameters between methane and TIP5P water are given

- Petrenko VF, Whitworth RW (1999) *Physics of Ice* (Oxford Univ Press, New York).
- Mishima O, Stanley HE (1998) The relationship between liquid, supercooled and glassy water. *Nature* 396:329–335.
- Mishima O, Calvert LD, Whalley E (1985) An apparently first-order transition between two amorphous phases of ice induced by pressure. *Nature* 314(6006):76–78.
- Hemley R, Chen L, Mao H (1989) New transformations between crystalline and amorphous ice. *Nature* 338(6217):638–640.
- Tse JS, et al. (1999) The mechanisms for pressure-induced amorphization of ice Ih. *Nature* 400(6745):647–649.
- Loerting T, Salzmann C, Kohl I, Mayer E, Hallbrucker A (2002) A second distinct structural "state" of high-density amorphous ice at 77 K and 1 bar. *Phys Chem Chem Phys* 3(24):5355–5357.
- Debenedetti PG, Stanley HE (2003) Supercooled and glassy water. *Phys Today* 56(6):40–46.
- Nelmes RJ, et al. (2006) Annealed high-density amorphous ice under pressure. *Nat Phys* 2(6):414–418.
- Loerting T, et al. (2006) Amorphous ice: Stepwise formation of very-high-density amorphous ice from low-density amorphous ice at 125 K. *Phys Rev Lett* 96(2):025702.
- Chen JY, Yoo CS (2011) High density amorphous ice at room temperature. *Proc Natl Acad Sci USA* 108(19):7685–7688.
- Debenedetti PG (1996) *Metastable Liquids* (Princeton Univ Press, Princeton).
- Mallamace F, et al. (2007) Evidence of the existence of the low-density liquid phase in supercooled, confined water. *Proc Natl Acad Sci USA* 104(2):424–428.
- Zhang Y, et al. (2011) Density hysteresis of heavy water confined in a nanoporous silica matrix. *Proc Natl Acad Sci USA* 108(30):12206–12211.
- Zangi R, Mark AE (2003) Monolayer ice. *Phys Rev Lett* 91(2):025502.
- Bai J, Angell CA, Zeng XC (2010) Guest-free monolayer clathrate and its coexistence with two-dimensional high-density ice. *Proc Natl Acad Sci USA* 107(13):5718–5722.
- Yang J, Meng S, Xu LF, Wang EG (2004) Ice tessellation on a hydroxylated silica surface. *Phys Rev Lett* 92(14):146102.
- Koga K, Zeng XC, Tanaka H (1997) Freezing of confined water: A bilayer ice phase in hydrophobic nanopores. *Phys Rev Lett* 79(26):5262–5265.
- Zangi R, Mark AE (2003) Bilayer ice and alternate liquid phases of confined water. *J Chem Phys* 119(3):1694–1700.
- Kumar P, Buldyrev SV, Starr FW, Giovambattista N, Stanley HE (2005) Thermodynamics, structure, and dynamics of water confined between hydrophobic plates. *Phys Rev E Stat Nonlin Soft Matter Phys* 72(5 Pt 1):051503.
- Giovambattista N, Rossky PJ, Debenedetti PG (2009) Phase transitions induced by nanoconfinement in liquid water. *Phys Rev Lett* 102(5):050603.
- Koga K, Tanaka H, Zeng XC (2000) First-order transition in confined water between high-density liquid and low-density amorphous phases. *Nature* 408(6812):564–567.
- Johnston JC, Kastelowitz N, Molinero V (2010) Liquid to quasicrystal transition in bilayer water. *J Chem Phys* 133(15):154516.
- Han S, Choi MY, Kumar P, Stanley HE (2010) Phase transitions in confined water nanofilms. *Nat Phys* 6(9):685–689.
- Bai J, Zeng XC, Koga K, Tanaka H (2003) Formation of quasi-two-dimensional bilayer ice in hydrophobic slit: A possible candidate for ice XIII? *Mol Simul* 29(10–11):619–626.
- Kimmel GA, et al. (2009) No confinement needed: Observation of a metastable hydrophobic wetting two-layer ice on graphene. *J Am Chem Soc* 131(35):12838–12844.
- Limmer DT, Chandler D (2011) The putative liquid-liquid transition is a liquid-solid transition in atomistic models of water. *J Chem Phys* 135(13):134503.
- Sciortino F, et al. (1995) Crystal stability limits at positive and negative pressures, and crystal-to-glass transitions. *Phys Rev E Stat Phys Plasmas Fluids Relat Interdiscip Topics* 52(6):6484–6491.
- Sloan ED, Jr. (2003) Fundamental principles and applications of natural gas hydrates. *Nature* 426(6964):353–363.
- Davidson DW, Handa YP, Ratcliffe CI, Tse JS, Powell BM (1984) The ability of small molecules to form clathrate hydrates of structure II. *Nature* 311:142–143.
- Ripmeester JA, Ratcliffe CI, Powell BM (1987) A new clathrate hydrate structure. *Nature* 325:135–136.
- Stern LA, Kirby SH, Durham WB (1996) Peculiarities of methane clathrate hydrate formation and solid-state deformation, including possible superheating of water ice. *Science* 273(5283):1843–1848.
- Walsh MR, Koh CA, Sloan ED, Sum AK, Wu DT (2009) Microsecond simulations of spontaneous methane hydrate nucleation and growth. *Science* 326(5956):1095–1098.
- Wang J, Yoo S, Bai J, Morris JR, Zeng XC (2005) Melting temperature of ice Ih calculated from coexisting solid-liquid phases. *J Chem Phys* 123(3):036101.
- Loveday JS, Nelmes RJ (2008) High-pressure gas hydrates. *Phys Chem Chem Phys* 10(7):937–950.
- Mahoney MW, Jorgensen WL (2000) A five-site model for liquid water and the reproduction of the density anomaly by rigid, nonpolarizable potential functions. *J Chem Phys* 112(20):8910–8922.
- Kesselring TA, Franzese G, Buldyrev SV, Herrmann HJ, Stanley HE (2012) Nanoscale dynamics of phase flipping in water near its hypothesized liquid-liquid critical point. *Sci Rep* 2:474–480.
- Ferguson AL, Giovambattista N, Rossky PJ, Panagiotopoulos AZ, Debenedetti PG (2012) A computational investigation of the phase behavior and capillary sublimation of water confined between nanoscale hydrophobic plates. *J Chem Phys* 137(14):144501.

Supporting Information

Bai and Zeng 10.1073/pnas.1213342110

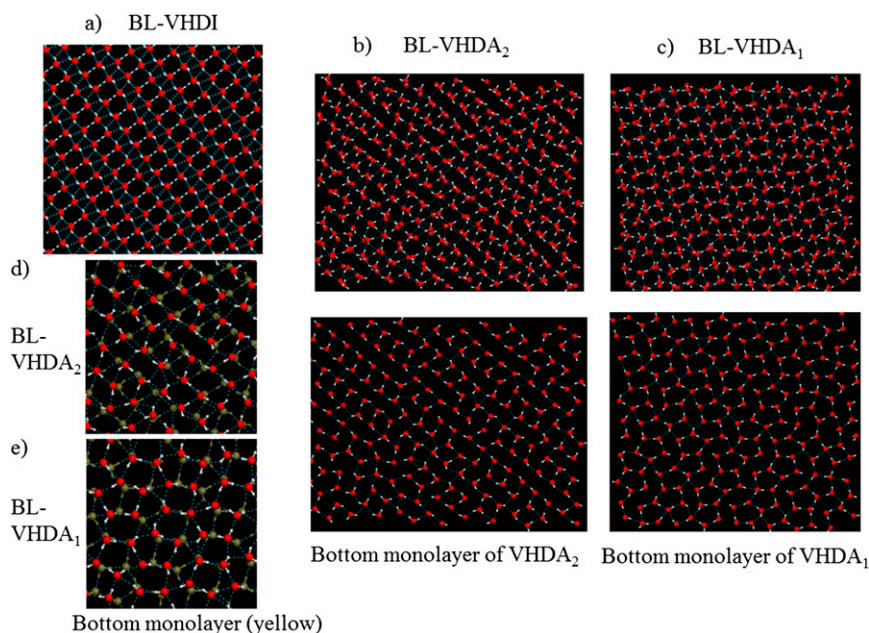


Fig. S1. (A) Hydrogen-bonding network of the bilayer very-high-density ice (BL-VHDI). Every water molecule in BL-VHDI interacts with its neighboring water molecules via six hydrogen bonds. (B) Top view of the bilayer very-high-density amorphous (BL-VHDA₂) ice, which is mostly composed of antistacked parallelograms (*Upper*); top view of the bottom monolayer of VHDA₂ (*Lower*). (C) Top view of the BL-VHDA₁, which is mostly composed of pentagons (*Upper*); top view of the bottom monolayer of VHDA₁ (*Lower*). The VHDA₁ can be obtained either by decompressing VHDA₂ ice or by cooling the liquid water under 2.0 GPa. The VHDA₁ exhibits structural similarity similar to BL-VHDI, but the hydrogen-bonding networks of the two are quite different. (D and E) Views are identical to B and C but replotted with the oxygen atoms of the bottom monolayer in yellow so that one can see more clearly how the two monolayers stack up.

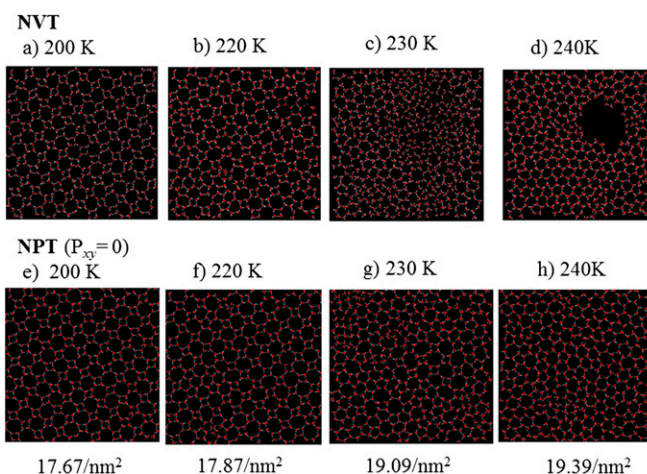


Fig. S2. Top views of a metastable bilayer low-density ice (BL-LDI, or guest-free bilayer methane clathrate) with the Archimedean 4-8² pattern, which is stable below 210 K. At 230 K, the BL-LDI transforms into a bilayer amorphous (BL-A) ice. Snapshots from *NVT* (A–D) and the constant particle number, lateral pressure, and temperature (*NP_{xy}hT*) (E–H) molecular dynamics simulations, respectively, show the transformation from BL-LDI to BL-A as the temperature increases from 200 to 240 K. The area density of water is given in E–H.

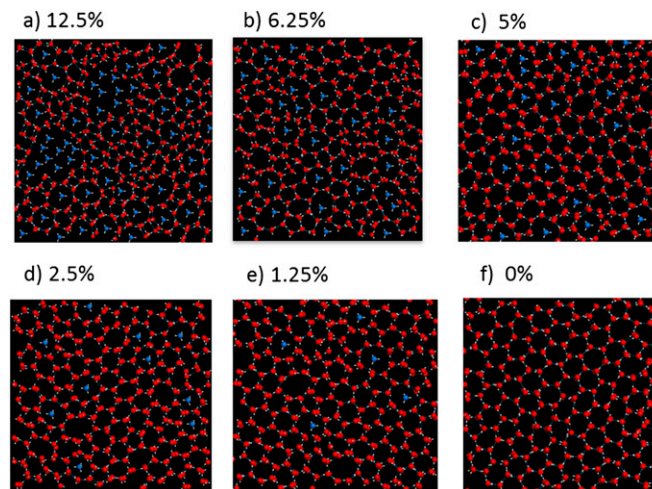


Fig. S3. Top views of snapshots of molecular dynamics (MD) simulation at different mole fractions of methane. All CH_4/water mixtures are equilibrated at 1,000 K and 0.5 GPa, and are then instantly quenched to 250 K at the same lateral pressure. Ratios of the number of methane and water molecules are 12.5% (A), 6.25% (B), 5% (C), 2.5% (D), 1.25% (E), and 0% (F). The total number of water molecules in the supercell is 400. The simulation time of each MD simulation is about 40 ns.

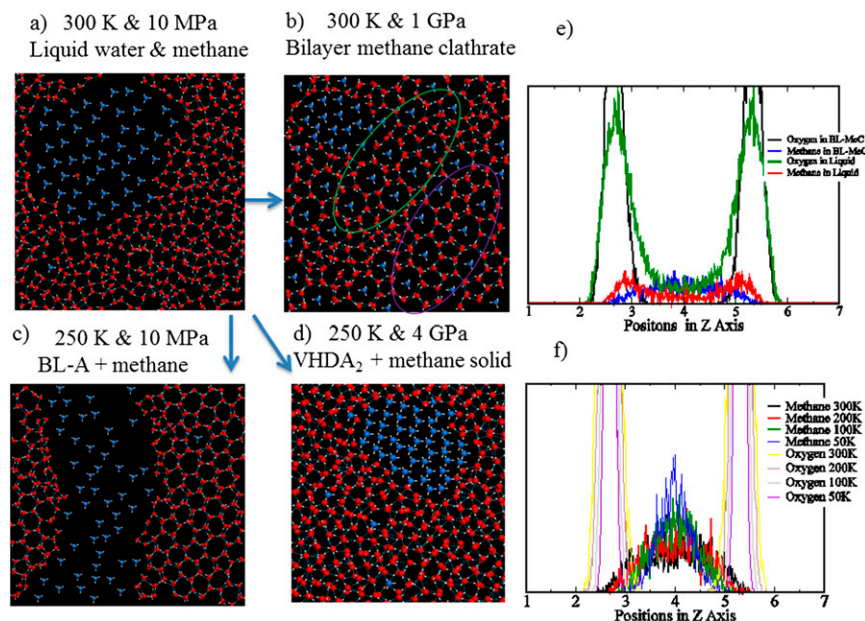


Fig. S4. (A) Top view of a snapshot of phase-separated methane and water at 300 K and 10 MPa. (B) Top view of a snapshot of the molecular dynamics (MD) simulation at 160 ns when the system in A is instantly compressed to 1 GPa (Movie S1). The green circle highlights the octagon-square domains. The purple circle highlights the methane-containing octagons connected by nexus pentagons. (C) View of a snapshot of the MD simulation at 60 ns when the system in A is instantly cooled to 250 K. (D) Top view of a snapshot of the MD simulation at 60 ns when the system in A is cooled and compressed instantly to 250 K and 4 GPa. The final structure is a mixture of ice amorphous with methane gas. (E) Density profiles of equilibrium bilayer methane clathrate (BL-MeC; at 0.1 MPa and 300 K) and phase-separated methane and water (10 MPa and 300 K). The green and red lines refer to density profiles of oxygen and methane, respectively, for the BL-MeC. (F) Density profiles of methane for the BL-MeC at 0.1 MPa and various temperatures [50 K (blue), 100 K (green), 200 K (red), and 300 K (black)] and density profiles of oxygen at various temperatures [50 K (purple), 100 K (gray), 200 K (brown), and 300 K (yellow)].

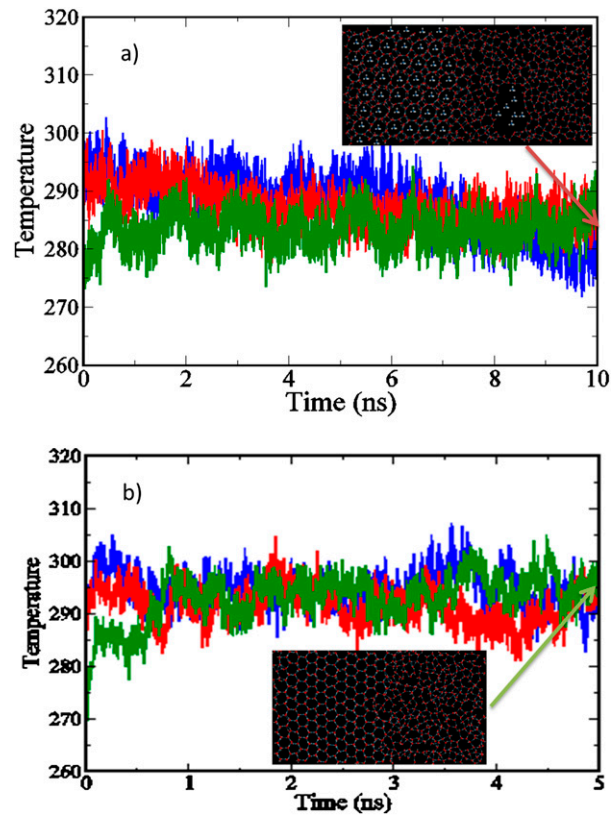
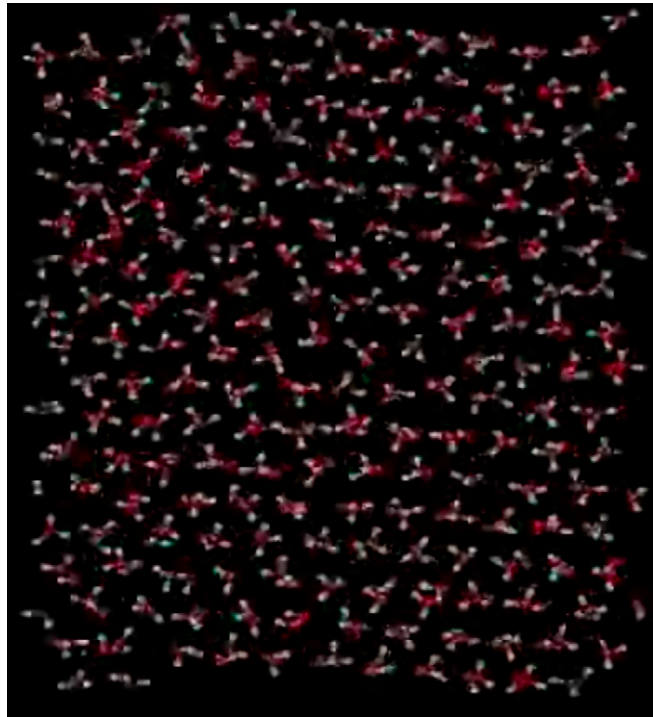
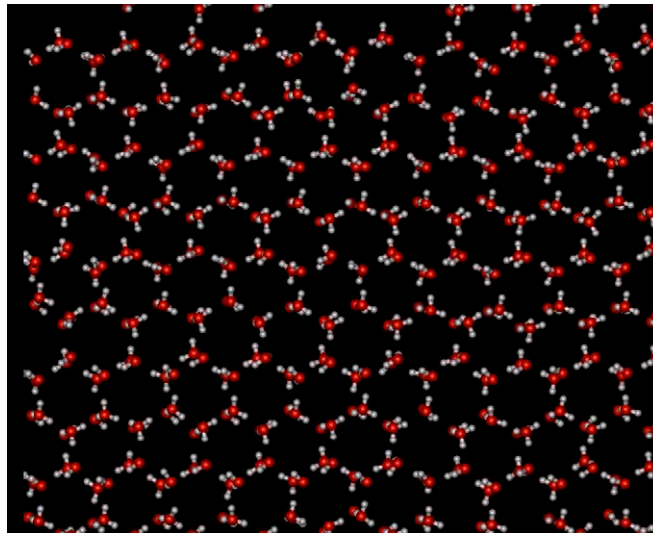


Fig. S5. Two-phase coexistence molecular dynamics simulations in the constant particle number, lateral pressure, and enthalpy ($NP_{xy}hH$) ensemble for the bilayer methane clathrate (BL-MeC) system (A) and bilayer ice-I (BL-ice I) system (B) at a constant lateral pressure (P_{xy}) = 1 bar. For the BL-MeC system, three systems (coexisting BL-MeC/water) are prepared, with the initial temperatures at 280 K, 290 K, and 300 K, respectively. For the BL-ice I system, three systems are prepared also, again with the initial temperatures at 270 K, 290 K, and 300 K, respectively. (Insets) Snapshots of the coexisting BL-MeC and liquid at 10 ns (A; with initial temperature at 290 K) and the coexisting BL-ice I and water at 5 ns (B; with initial temperature at 270 K).



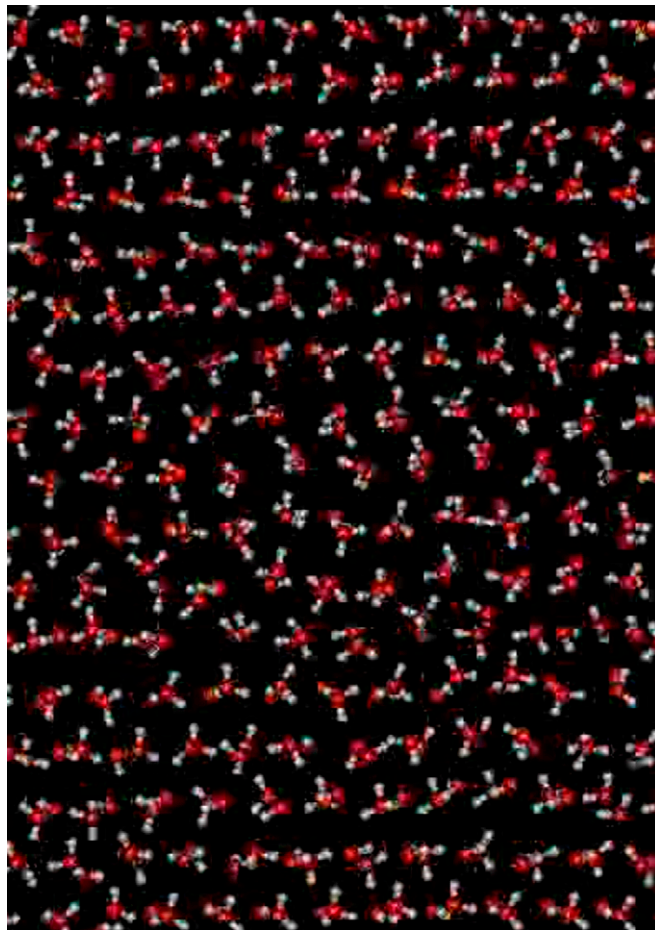
Movie S1. Molecular dynamics simulation of very-high-density amorphous (VHDA) ice (VHDA₂ → VHDA₁) transition.

[Movie S1](#)



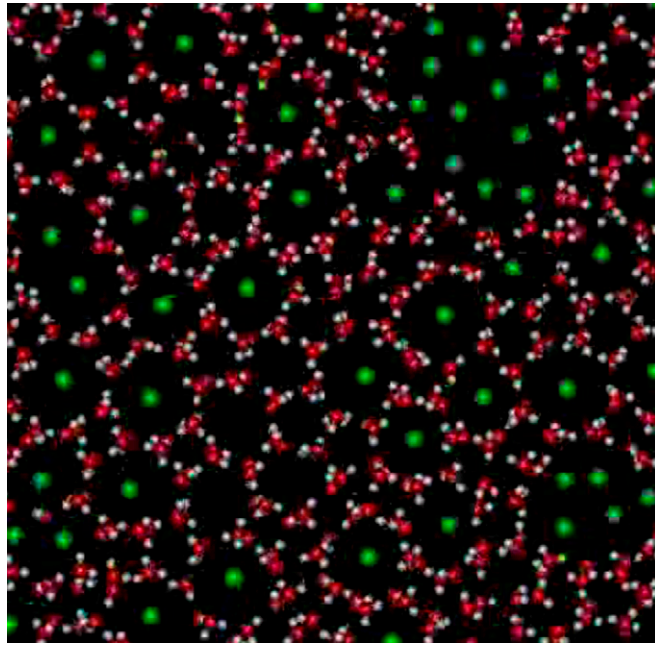
Movie S2. Molecular dynamics simulation of bilayer (BL)-ice I to BL-very-high-density crystalline ice (VHDI).

[Movie S2](#)



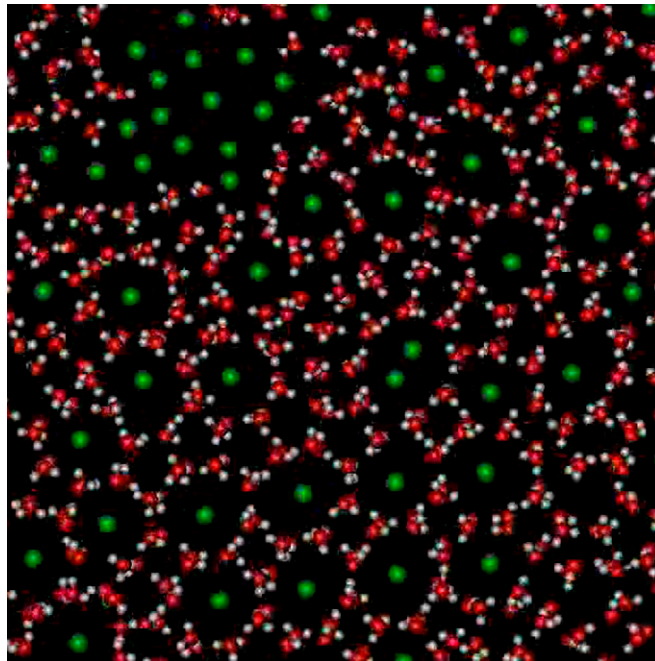
Movie S3. Molecular dynamics simulation of bilayer (BL)-ice I to very-high-density amorphous (VHDA₂) ice transition, where the Oswald staging phenomenon is shown.

[Movie S3](#)



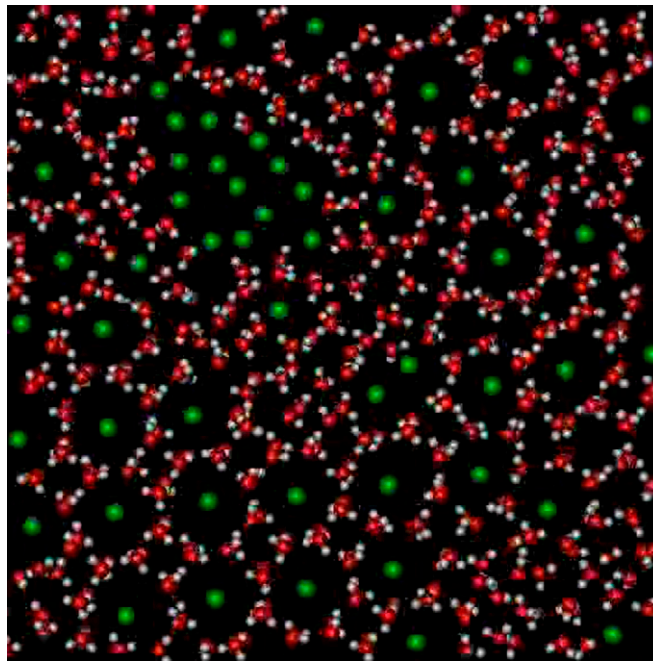
Movie S4. Molecular dynamics simulation of quench of a bilayer water/CH₄ mixture, where the composition of CH₄ is 12.5%.

[Movie S4](#)



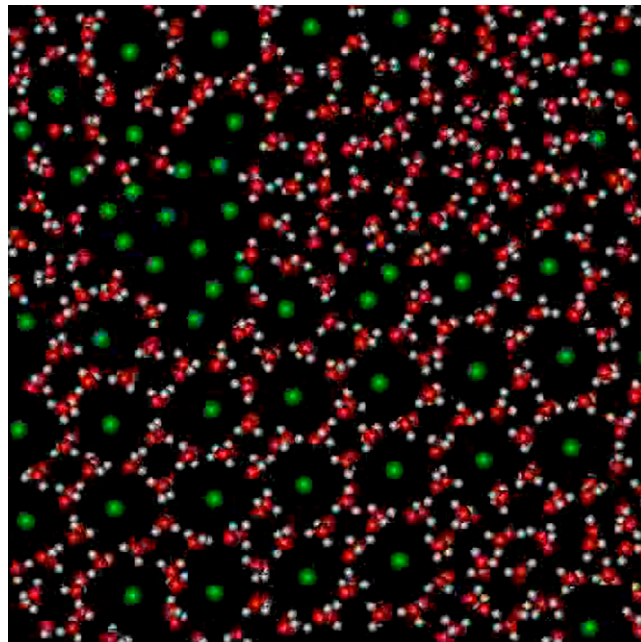
Movie S5. Molecular dynamics simulation of a bilayer water/CH₄ mixture, where the composition of CH₄ is 12.5%, temperature = 300 K, and constant lateral pressure (P_{xy}) = 1 GPa.

[Movie S5](#)



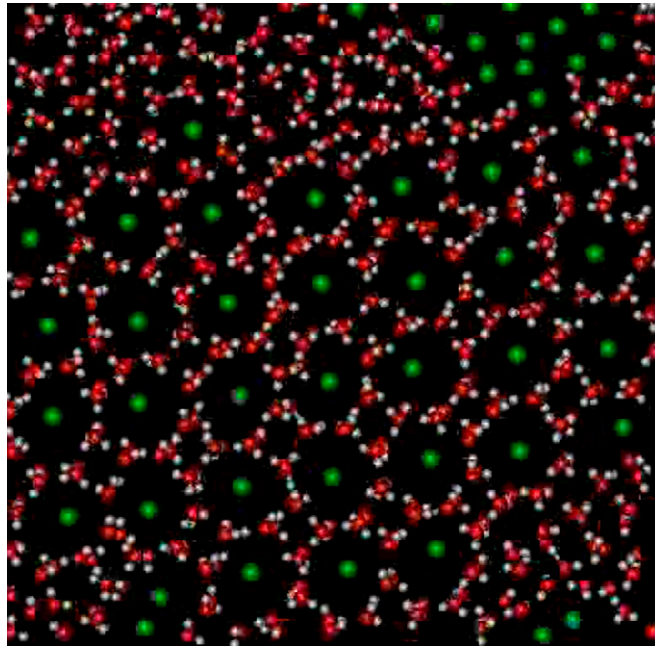
Movie S6. Molecular dynamics simulation of a bilayer water/CH₄ mixture, where the composition of CH₄ is 12.5%, temperature = 310 K, and constant lateral pressure (P_{xy}) = 1.5 GPa.

[Movie S6](#)



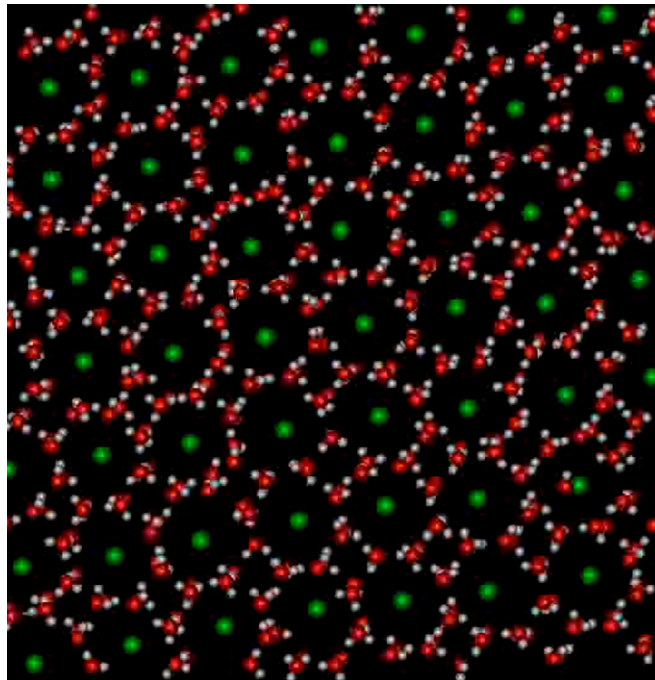
Movie S7. Molecular dynamics simulation of a bilayer water/CH₄ mixture, where the composition of CH₄ is 12.5%, temperature = 320 K, and constant lateral pressure (P_{xy}) = 1.5 GPa.

[Movie S7](#)



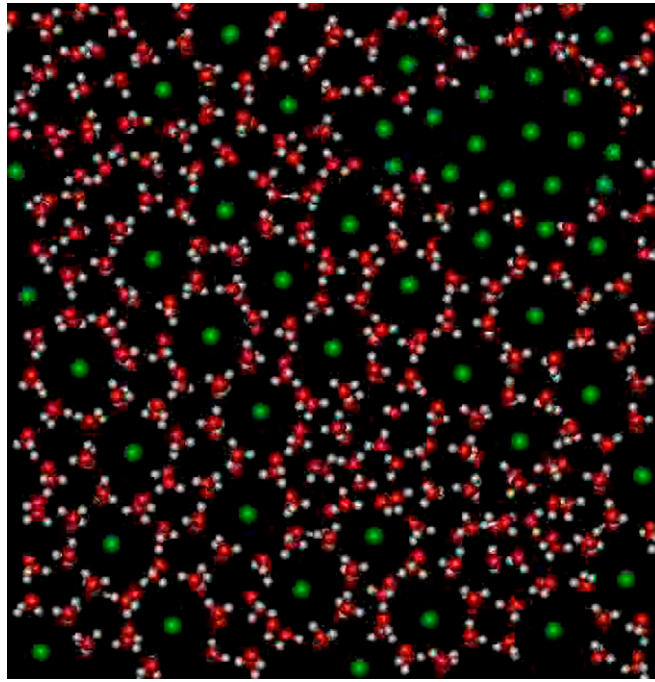
Movie S8. Molecular dynamics simulation of a bilayer water/CH₄ mixture, where the composition of CH₄ is 12.5%, temperature = 325 K, and constant lateral pressure (P_{xy}) = 1.5 GPa.

[Movie S8](#)



Movie S9. Molecular dynamics simulation of a bilayer water/CH₄ mixture, where the composition of CH₄ is 12.5%, temperature = 325 K, and constant lateral pressure (P_{xy}) = 1 GPa.

[Movie S9](#)



Movie S10. Molecular dynamics simulation (160 ns) of a bilayer water/CH₄ mixture, where the composition of CH₄ is 12.5%, temperature = 300 K, and constant lateral pressure (P_{xy}) = 1 GPa.

[Movie S10](#)